JACS
JOURNAL OF THE AMERICAN CHEMICAL SOCIETY

ARTICLE

pubs.acs.org/JACS

Ionic-Charge Dependence of the Intermolecular Coulombic Decay Time Scale for Aqueous Ions Probed by the Core-Hole Clock

Wandared Pokapanich,[†] Nikolai V. Kryzhevoi,[*,‡] Niklas Ottosson,[†] Svante Svensson,[†] Lorenz S. Cederbaum,[‡] Gunnar Öhrwall,[¶] and Olle Björneholm[*,†]

[†]Department of Physics and Astronomy, Uppsala University, P.O. Box 516, SE-751 20 Uppsala, Sweden

[‡]Theoretische Chemie, Physikalisch-Chemisches Institut, Universität Heidelberg, Im Neuenheimer Feld 229, D-69120 Heidelberg, Germany

[¶]MAX-lab, Lund University, P.O. Box 118, SE-221 00 Lund, Sweden

Supporting Information

ABSTRACT: Auger electron spectroscopy combined with theoretical calculations has been applied to investigate the decay of the Ca 2p core hole of aqueous Ca^{2+}. Beyond the localized two-hole final states on the calcium ion, originating from a normal Auger process, we have further identified the final states delocalized between the calcium ion and its water surroundings and produced by core level intermolecular Coulombic decay (ICD) processes. By applying the core-hole clock method, the time scale of the core level ICD was determined to be 33 ± 1 fs for the 2p core hole of the aqueous Ca^{2+}. The comparison of this time constant to those associated with the aqueous K^+, Na^+, Mg^{2+}, and Al^{3+} ions reveals differences of 1 and up to 2 orders of magnitude. Such large variations in the characteristic time scales of the core level ICD processes is qualitatively explained by different internal decay mechanisms in different ions as well as by different ion−solvent distances and interactions.

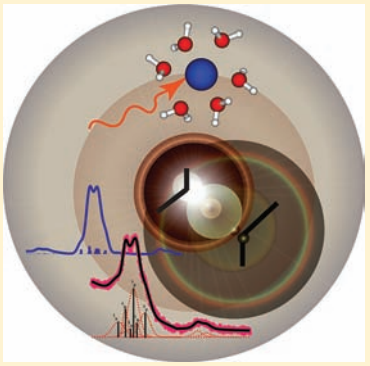

INTRODUCTION

Auger electron spectroscopy (AES) is a powerful technique for investigating the local atomic environment in all phases of matter, that is, solid, gaseous, or liquid. An Auger process can be considered as involving two basic steps, illustrated in Figure 1. The first step is the removal of an electron from an inner, atomic-like, core level upon absorption of an X-ray photon. From this valence-electronically (but not geometrically) relaxed core-hole state, the second step starts. The core hole is filled by an electron from a higher level, while another electron is ejected. Alternatively to the irradiative Auger decay, the core hole may decay radiatively by emission of a photon. For shallow core levels, the irradiative channel is strongly dominating.

The interatomic or intermolecular Coulombic decay (ICD) process is another irradiative channel, in which one of the final state holes is located on a site different from the originally core-ionized one, see Figure 1. ICD was first predicted and observed for inner valence holes in van der Waals-bonded systems,[1−3] where it operates in the low femtosecond (fs = 10^{-15} s) time scale.[4,5] No signature of ICD-like processes of deeper, core level vacancies in van der Waals-bonded systems has been found yet, and the Auger process is thus the only irradiative decay observed in these systems.[6] In contrast, in systems bound by hydrogen bonds, ICD operative both in inner valence[1,7−10] and in core level[11−14] regimes has been observed. Auger and core level ICD-like (hereafter for brevity ICD) processes are schematically shown in Figure 1a together with the energy relations between the involved states (see Figure 1b).

The core-hole clock is an effective method to investigate charge transfer dynamics.[15,16] This technique is based on using the relatively well-known lifetime of a core hole as an internal reference to time another, parallel dynamic process observed as a separate channel in the core-hole decay spectrum. The relaxation of a core-hole state can for instance be probed by investigating Auger and ICD processes. For very fast charge transfer processes, the Coster−Kronig (CK) decay, in which the initial and final vacancies are in the same electronic shell, can be used as the internal reference.[17]

Typically, the core-hole lifetime of levels accessible in soft X-ray spectroscopy are on the low femtosecond time scale. In a previous work,[12] we investigated the electronic decay of the K 2p hole in aqueous KCl and in microsolvated $KCl(H_2O)_n$ clusters and found both localized and delocalized final states produced via Auger and ICD mechanisms, respectively. In this work, we present combined X-ray photo and Auger electron spectroscopy (XPS and AES) results for the 2p core-hole decay of Ca^{2+} in aqueous $CaCl_2$ solution together with theoretical simulations of the Auger spectra of microsolvated $Ca^{2+}(H_2O)_n$ clusters. Just as for K^+_{aq},[12] Auger and ICD final states are found in these systems too. The results obtained are used to determine the time scale of the ICD processes in the aqueous solutions using the core-hole clock and to explore its dependences on the ionic charge and on the ion−solvent distances and interactions.

Received: April 14, 2011
Published: July 28, 2011

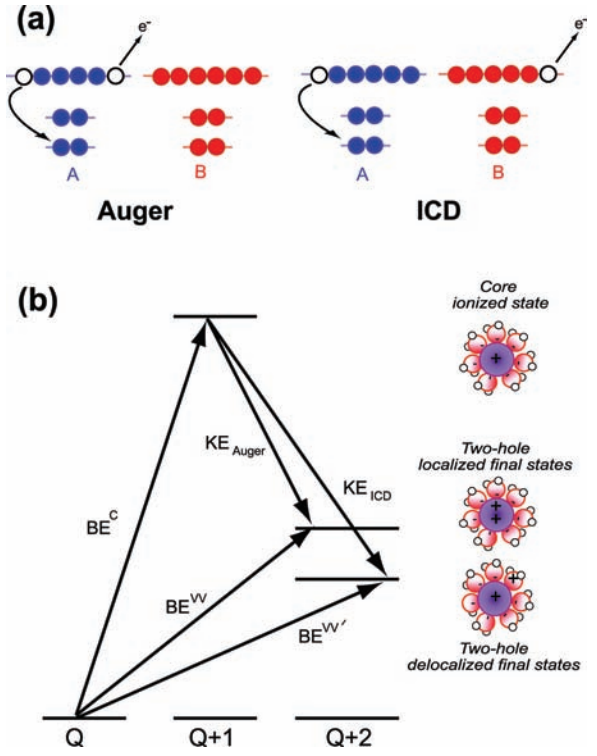

Figure 1. Schematic figure of the Auger and core level ICD process (a), and energy relations between the involved states for an ion of initial charge Q (b). The Auger and ICD electron energies (KE_{Auger} and KE_{ICD}) are the difference between the core binding energy (BE^{C}) and the energy of the two-hole final states BE^{VV} and $BE^{VV'}$ which refer to localized and delocalized final states, respectively.

Recently, the ICD lifetimes upon formation of a $2s^{-1}$ state in the aqueous Na^+, Mg^{2+}, and Al^{3+} were estimated.[18] These were found to be 1 and up to 2 orders of magnitude shorter than the ICD lifetimes of the aqueous Ca^{2+} and K^+, $2p^{-1}$ state. Such dramatic differences in the ICD lifetimes deserve particular attention, and are in the present study attributed to different internal decay mechanisms in the respective solvated ions.

EXPERIMENTAL SECTION

The experiments were performed using the liquid jet technique, which has completely revolutionized the field of electron spectroscopy of liquids.[19] We investigated the core-hole decay of Ca^{2+} in aqueous $CaCl_2$, by concentrating on the intensity ratio between the delocalized and localized final states. Aqueous $CaCl_2$ was prepared by mixing the high purity salt (≥99.0%, Sigma Aldrich) with deionized water to obtain concentration of 1.0 *m*.

The core level Ca^{2+} 2p photoelectron and Auger electron spectra were recorded with the same photon energy of 400 eV. The valence Ca^{2+} 3p spectrum was recorded with the photon energy of 100 eV. The binding energies were calibrated relative to the valence X-state of liquid water, at 11.16 eV.[20] The experiment was performed at the Swedish synchrotron radiation facility MAX-lab. The undulator-based soft X-ray beamline I411[21,22] using a Scienta R4000 electron spectrometer was mounted at the magic angle 54.7° in order to avoid angular effects. The total experimental resolution was controlled by the photon bandwidth and the spectrometer; both core and valence regions were estimated to be 60 and 170 meV, respectively. For the Ca^{2+} 2p Auger spectrum, the photon bandwidth is of no importance; it was 250 meV. The experimental spectrum was fitted by taking Gaussian and Lorenzian contributions into account, as well as a post collision interaction for the finite lifetime of the core hole and the interaction between the photoelectron and the Auger electron emitted in the deexcitation of the core-hole state. The systematic error in Auger spectrum varied due to the fluctuated fitting.

The spectra were recorded using a liquid jet with a diameter of 15 μm injected into a differentially pumped vacuum chamber. The propagation of the jet was perpendicular to the direction of the photon beam in the spectrometer. Typical working pressures were in the 10^{-5} mbar range in the differential pumping stage and in the 10^{-6} mbar range in the analyzer chamber. The downstream velocity of the jet was 60 m/s. The experimental setup has been described in more detail elsewhere.[23]

COMPUTATIONAL DETAILS

Like in our previous study on the aqueous KCl solution,[12] we provide a theoretical support for the experimental Auger spectrum. Again, microsolvated clusters were chosen as model systems. Although the correct absolute energies of electronic transitions in liquid can hardly be obtained by using such systems (long-range interactions between the solvated ion and solvent molecules beyond the first solvation shell should be taken into account to reproduce the gas-to-liquid energy shifts), the overall shape of the Auger spectrum can reliably be reproduced in the framework of the finite-size microsolvated model as will be seen below.

In contrast to ref 12 where microsolvated clusters with both the K^+ and Cl^- counterions present at the same time were considered, here, we ignore the presence of the Cl^- anions. In the aqueous $CaCl_2$ solution under study, most of the ion pairs are expected to be solvent separated, and as such, the impact of Cl^- on the shape of the Auger spectrum of Ca^{2+} is insignificant.

The considered clusters represent fully symmetric systems of mono-, di-, tetra-, and hexahydrated calcium dications (computational limitations prohibit considering larger clusters). Their geometries were optimized at the level of second-order Møller−Plesset perturbation theory using the 6-311++G(2d,2p) basis sets[24] for all the atoms. The geometry optimization was carried out without freezing any orbitals. We mention that the computed characteristic distances between Ca^{2+} and the oxygen atoms increase with growing cluster size and constitute 2.265, 2.312, 2.348, and 2.401 Å in the clusters of Ca^{2+} with one, two, four, and six water molecules in the first solvation shell, respectively. Note that in the microsolvated $K^+(H_2O)_n$ clusters, whose geometries were also optimized at the same level of theory, the respective ion−water separations are noticeably larger (2.638, 2.676, 2.713, and 2.760 Å for n = 1, 2, 4, and 6, respectively) as a consequence of weaker ion−water interactions.

The double ionization potential (DIP) scale is used to compare the experimental and theoretical Auger spectra. The DIPs of the clusters have been computed by means of the second order algebraic diagrammatic construction method, ADC(2),[25,26] which is an all-electron *ab initio* Green's function method. We used relativistic pseudopotental basis sets[27,28] augmented with a *d*-type polarization and *s*- and *p*-type diffuse functions for the heavy atoms. A double-ζ quality basis set[29] was taken for the hydrogen atoms.

A two-hole population analysis[30] enables us to represent the transition moments between the N-particle ground and N − 2-particle final states and thus the heights of all the computed spectral lines as sums of various contributions characterized by different localizations of the final holes on different atomic sites in the system. Interested in the Auger spectrum of Ca^{2+}, we selected only those contributions which are associated with two final holes localized on the calcium dication. The fact that the experimental spectrum describes Auger transitions from the spin−orbit split initial Ca $2p^{-1}$ core hole state was taken into account in the theoretical simulations. We split each line in the calculated spectra

into two lines corresponding to the final Auger L_2 and L_3 states with the intensity ratio 1:1.5. The energy splitting is chosen to be 3.8 eV according to the spin−orbit splitting of the Ca $3p^{-1}$ level in the $CaCl_2$ aqueous solution (see below). In the end, all the individual lines were convoluted uniformly with a Gaussian with a full width at half-maximum (fwhm) parameter of 3 eV that results in nearly the same widths of the principal Auger features in the theoretical and experimental spectra.

RESULTS AND DISCUSSION

The Binding Energy of 2p and 3p Holes of the Aqueous Ca^{2+}. In the core-hole decay processes schematically shown in Figure 1, the initial state energy of the core-hole decay equals the 2p binding energy (BE). The final state of the core-hole decay processes contains one or two holes in 3p, and the final state energy thus depends on the 3p BE. For these reasons, the 2p and 3p photoelectron spectra of aqueous Ca^{2+} were recorded, and the spectra are shown in Figure 2, panels a and b, respectively. The obtained vertical BEs are 356.6 and 352.8 eV for the Ca^{2+} $2p_{1/2}$ and $2p_{3/2}$ states, respectively, whereas the Ca^{2+} 3p vertical BE is 29.8 eV.

The 2p Core-Hole Decay Spectrum of the Aqueous Ca^{2+}. The $L_{2,3}M_{2,3}M_{2,3}$ Auger spectrum of the aqueous Ca^{2+} is seen in Figure 3 in the 275−300 kinetic energy (KE) interval. Its overall appearance is similar to that of solid $CaCl_2$ and CaF_2.[31,32] As seen in Figure 2a, the core-hole decay starts from two spin−orbit split Ca 2p core-hole states, and leads to two holes in the 3p shell. The resulting $3p^{-2}$ configuration created via Auger decay gives rise to three different final states ^1S, ^1D, and ^3P states, resulting in two sets of three transitions each. As the first step in the analysis, we have therefore fitted the $L_{2,3}M_{2,3}M_{2,3}$ spectral feature with two series of peaks corresponding to the $L_2M_{2,3}M_{2,3}$ and $L_3M_{2,3}M_{2,3}$ transitions. The intensities of the $L_2M_{2,3}M_{2,3}$ lines were set to half of the $L_3M_{2,3}M_{2,3}$ ones. The energy differences between the related lines from the two sets were fixed to 3.8 eV, which corresponds to the Ca 2p spin−orbit splitting obtained from the XPS spectrum. The kinetic energies obtained from the Auger spectrum fitting for the $L_3M_{2,3}M_{2,3}$ ^3P, ^1D, and ^1S states are 287.9, 285.3, and 283.1 eV, respectively, as shown in Figure 3.

The Ca^{2+} Auger spectrum also exhibits a weak but distinct feature located between 303 and 315 eV KE as seen in Figure 3. Two peaks, again separated by 3.8 eV, were used to fit this feature. Its kinetic energy does not depend on the photon energy, indicating that it results from an electronic decay process. The fact that this feature has a kinetic energy higher than the main $L_{2,3}M_{2,3}M_{2,3}$ feature suggests that one of the involved final vacancies resides on a neighboring to Ca^{2+} site, and consequently that the electronic decay process in question is ICD. Aqueous $CaCl_2$ solution is regarded to not contain contact ion pairs, even at much higher concentrations than studied here, though solvent-shared ion pairs may exist.[33,34] It is therefore expected that the high KE spectral feature is not due to the presence of chloride anions in the solution but rather its appearance is attributed to the final states involving holes on calcium and water.

The DIPs of such delocalized two-hole final states can be estimated using the known one-hole BEs for the Ca^{2+} $3p^{-1}$ and water $(1b_1)^{-1}$ (X), $(3a_1)^{-1}$ (A), and $(1b_2)^{-1}$ (B) states, see the expanded spectrum in the inset of Figure 3. One extreme is to treat the two holes as independent, that is, assuming that they are completely screened and/or infinitely far apart. In this case, the DIP is the sum of two one-hole BEs. Such DIPs form the minimum, low-energy ends of the two-hole final state intervals shown. The maximum, high DIP ends are instead obtained by accounting for the mutual Coulomb repulsion between the neighboring holes. The mean Ca−O distance of 2.46 Å[35] gives a Coulomb energy of 17.55 eV. When the upper and lower DIP limits are combined, we obtain two-hole final state energy

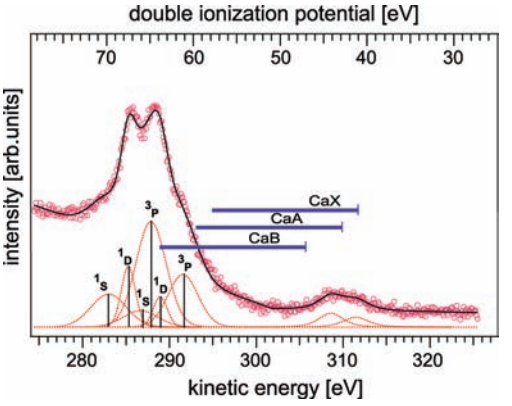

Figure 3. The Ca^{2+} Auger spectrum of aqueous $CaCl_2$. The $L_{2,3}M_{2,3}M_{2,3}$ features corresponding to the transitions from the spin−orbit split Ca^{3+} $2p^{-1}$ initial state to the Ca^{4+} $3p^{-2}$ final localized states are seen in the kinetic energy range from approximately 276 to 297 eV. The dashed lines show the individual fitted peaks. The solid line gives the resulting fit envelope. The solid vertical bars represent the centers of gravity of the multiplet components. The feature located at the KEs from about 303 to 315 eV corresponds to the transitions from the Ca^{3+} $2p^{-1}$ initial state to the Ca^{3+} $3p^{-1}$ + water valence vacancy final delocalized states. This spectral feature is fitted by two peaks. The horizontal solid lines show the estimated energy ranges for the two-hole final CaX, CaA, and CaB states (see text for notations).

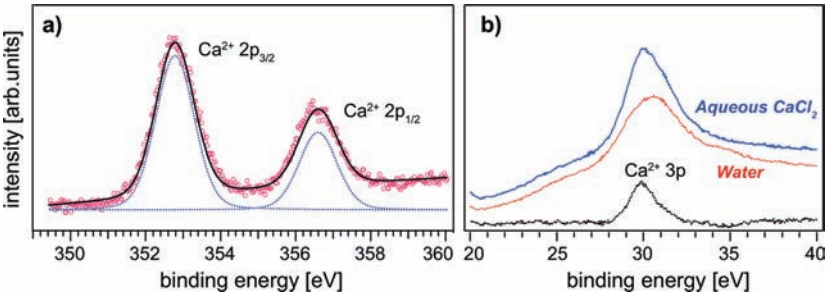

Figure 2. Photoelectron spectra of the aqueous Ca^{2+} 2p (a) and 3p (b) levels. In the core photoelectron spectrum, the dotted lines show the individual fitted peaks. The solid line gives the resulting fit envelope. The valence spectrum of Ca^{2+} is obtained as the difference between the spectra of the aqueous calcium chloride and liquid water.

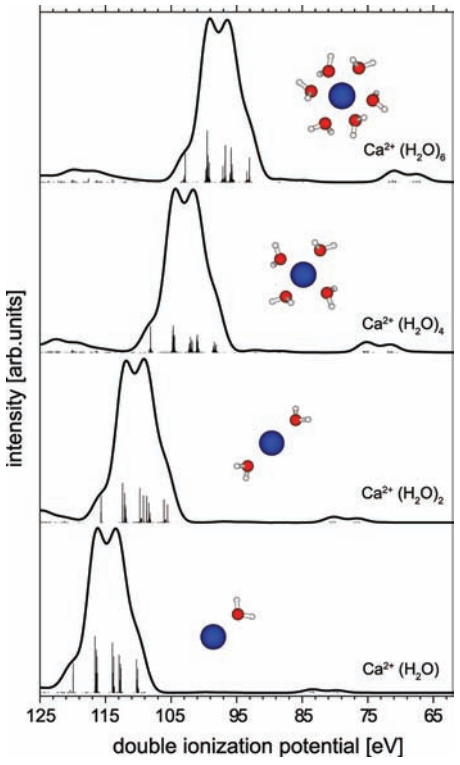

Figure 4. The computed Auger spectra of the microhydrated calcium dication. The most intense features are associated with the final Auger states where both outer valence vacancies are localized on calcium. At lower DIPs, one sees spectral features growing with cluster size which corresponds to the ICD states. Here, one outer valence vacancy is localized on calcium, the other on water molecules. The intensity ratios between the ICD and Auger spectral features are shown in Figure 5.

intervals for Ca $(3p)^{-1}$ H_2O $(1b_1)^{-1}$, Ca $(3p)^{-1}$ H_2O $(3a_1)^{-1}$, and Ca $(3p)^{-1}$ H_2O $(1b_2)^{-1}$ (denoted CaX, CaA, and CaB) of 41.16−58.71, 43.50−61.05, and 47.34−64.89 eV, respectively, as shown by horizontal bars in Figure 3. As seen, the lower DIP limits of these energy intervals overlap well with the observed feature. We therefore interpret these features to arise from an ICD processes, transforming the $2p^{-1}$ core-hole state of Ca^{2+} to delocalized final states with one Ca 3p vacancy and one vacancy on a neighboring water molecule. We note that in both the O 1s decay spectrum of water clusters and the K 2p decay spectrum of aqueous potassium chloride, the final states delocalized over two centers were found to have DIPs close to those expected from a simple addition of the single-hole BEs, indicating that the ions in the aqueous environment are efficiently screened,[11,12] or that the holes on the water predominately are in the HOMO orbital.

Auger Spectra of Microsolvated Ca^{2+}. Figure 4 displays the calculated Auger spectra of a series of microsolvated $Ca^{2+}(H_2O)_n$ (n = 1, 2, 4, 6) clusters. The correspondence between these spectra and the experimental Auger spectrum of aqueous Ca^{2+} shown in Figure 3 can easily be established. Each spectrum exhibits a very intense main feature originating from final Auger states with both the two outer valence holes localized on the initially core-ionized calcium ion. A much weaker feature is seen at lower DIPs. The two-hole population analysis clearly identifies the states contributing to this feature as being delocalized, with one hole on the initially core-ionized calcium ion and the other on a surrounding water. As seen in Figure 4, DIPs associated with the Auger and ICD processes are lowered with sequentially increasing hydration as a result of increasing charge-dipole and polarization interactions. The relative energy between the features resulting from Auger and ICD decreases, however, since the higher charge on the Ca^{4+} ion in the localized final Auger states exerts a considerably larger polarization effect on water molecules and interacts more strongly with water dipoles than the more extended charge distribution of the Ca^{3+} and H_2O^+ ions in the delocalized final ICD states. The Auger feature thus moves toward lower DIP faster.

The absolute energies of the spectral features deserve attention. A comparison of the experimental DIPs of the aqueous Ca^{2+} with those of the bare Ca^{2+} reveals a chemical shift of about −52 eV. The corresponding value for K^+ is about −25 eV[12] and thus 2.1 times smaller. Note that a model which considers only polarization interaction as the origin of the chemical shift and assumes the same ion−water distances in the aqueous Ca^{2+} and K^+ predicts the ratio of the two chemical shifts of 1.5. The ion−water separations in the aqueous solutions considered are however different. For example, the distances from calcium to the waters in the first solvation shell are 2.40−2.46 Å.[34−37] The respective values in the case of potassium are 2.65−2.90 Å.[36,38−40] Both ions likely have the same number of the nearest neighbor water molecules (6−8, according to experimental and theoretical studies[34−40]).

The differences in the first solvation shell around the ions alone, however, cannot explain the relatively large ratio of the chemical shifts. This is seen from our calculations on the hexahydrated calcium and potassium clusters which exhibit a similar relation between the ion−water distances as in the bulk solutions (see Computational Details). Microhydration of Ca^{2+} in six water molecules gives rise to a lowering of the DIPs by 23 eV while the presence of six water molecules around K^+ reduces the DIPs of this ion by 14 eV. The ratio of the two chemical shifts is thus only 1.6. Apparently, the water structure beyond the first solvation shell exerts a further profound effect on the chemical shift.

The second solvation shell around an aqueous potassium cation is not very pronounced and no evidence of a third solvation shell was found.[39] A contribution into the chemical shift due to the ion−water dipole interaction in such a relatively disordered structure is expected to be small since positive and negative contributions largely cancel. Contrastingly, an aqueous calcium dication exhibits a well-defined second solvation shell with water molecules aligned to the ionic field,[34,35] and moreover, a third solvation shell can be identified. Since the number of water molecules in these shells is large, this makes the impact of the long-range ion-dipole interaction there, in spite of large ion−water separations, comparable to that due to the first solvation shell and the chemical shifts in the Auger spectrum of the aqueous Ca^{2+} get considerably enhanced.

The ICD Time Scale for Aqueous KCl and $CaCl_2$. The relative intensity of the different core-hole decay channels, namely, the ICD channel leading to delocalized two-hole states and the Auger channel leading to localized two-hole states, is proportional to the relative decay rates, and thus inversely proportional to the respective decay lifetimes. We can thus use the core-hole clock method to establish the ICD time scale τ_{ICD} by using the relatively well-known time scale τ_{Auger} of the normal Auger decay.[16,41]

To explore this for both mono and divalent cations, we fitted the K^+ core-hole decay spectrum from ref 12 analogously to the

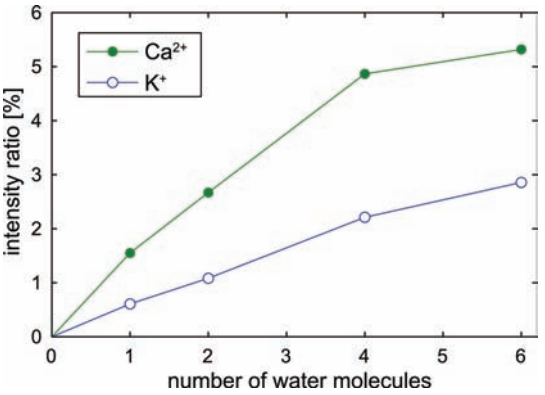

Figure 5. The intensity ratio of the delocalized ICD to localized Auger final states after the 2p core hole decay as a function of the number of water molecules in the microsolvated K^+ and Ca^{2+} clusters.

present Ca^{2+} case, and calculated the intensity ratios between the delocalized and localized final states for both the cations. The fractions between the two channels in the aqueous K^+ and Ca^{2+} are $1.9 \pm 0.1\%$ and $9.5 \pm 0.3\%$, respectively. Note that the errors were estimated from the fitting. The τ_{Auger} of K^+ and Ca^{2+} have been taken from data for the free molecules KCl and CaF_2, for which they are approximately 3.7 and 3.1 fs, respectively.[31,42] Therefore, K^+ and Ca^{2+} in aqueous solutions have the $2p^{-1}$ ICD decay time scale of roughly 195 ± 10 and 33 ± 1 fs, respectively.

We have further computationally investigated the relative importance of the ICD and Auger channels for K^+ and Ca^{2+} as a function of the number of solvent water molecules (see Figure 5). The first observation is that, with increasing number of water molecules, the relative efficiency of the ICD process also increases. This is an expected behavior, as the number of available open ICD channels grows with each new water molecule added to the system (see, e.g., refs 4, 43), while the Auger rate remains essentially constant. Noteworthy, the ICD efficiency is not proportional to the number of water molecules but rather increases only weakly sublinearly with the solvation degree. This is due to the ion−water distances in the clusters increasing with cluster size.

The second observation is that the divalent Ca^{2+} cation has a stronger effect than the monovalent K^+ cation, in the sense of yielding higher ICD fractions and thus shorter ICD lifetimes, in agreement with the experiment. This is also understandable. The ionic radius of Ca^{2+} and K^+ are 0.99 and 1.33 Å, respectively.[44,45] The smaller size and double charge of Ca^{2+} leads to a stronger electric field, resulting in a stronger ion−water bonding and a shorter ion−water distance for Ca^{2+} than for K^+. A smaller ion−water distance implies a larger overlap between the ion and water orbitals, facilitating the ICD process.[46] Moreover, the positive ionic charge induces a polarization of the water molecules, which increases the electron density on the oxygen atom facing the cation. This increase of electron density in the vicinity of the ion, which occurs already in the ground state, also facilitates the ICD process. Additionally, the electronic structure and thus the ICD efficiency is affected by the polarization of the surrounding water molecules induced by the intermediate core-ionized Ca $(2p^{-1})^{3+}$ and K $(2p^{-1})^{2+}$ states.

One sees from Figure 5 that the theoretical values associated with the calcium dication are 2−2.5 times larger than the respective values associated with the potassium cation in the mirosolvated clusters. The experimentally derived ratio for the two aqueous ions is 5. This trend can be understood by studying microsolvated clusters. The discrepancy arises due to several reasons. The main reason is believed to be connected to the effect of the water molecules beyond the first solvation shell which is missing in the microsolvated clusters. That the impact of the second and further coordination shells on the ICD efficiency can be substantial is seen, for example, from ref 43 where an example of a much less inert helium environment was considered. The fact that aqueous Ca^{2+} has a more compact and more ordered water network beyond the first solvation shell than aqueous K^+ does enhances the ICD efficiency in the calcium case and thus qualitatively explains its 5-fold increase relative to the potassium case.

The ICD Time Constants of Aqueous Multicharged Ions. In addition to the aqueous K^+ and Ca^{2+} ions, ICD has also been reported for the aqueous Na^+, Mg^{2+} and Al^{3+} ions.[18] By analyzing the broadenings of the 2s photoelectron lines of these ions, the ICD processes have been shown to operate on a much shorter time scale than in the above-discussed K^+ and Ca^{2+} cases, namely, 3.1 fs for Na^+, 1.5 fs for Mg^{2+}, and 1.0 fs for Al^{3+}.

As discussed above, the ionic charge has a strong influence on the ICD time scale. It is therefore reasonable to compare ions of equal charge, that is, Na^+ to K^+ and Ca^{2+} to Mg^{2+}. The ratio between the ICD lifetimes is 40 for K^+/Na^+ and 16 for Mg^{2+}/Ca^{2+}. These large ratios are difficult to explain by only the small differences in the solvation numbers and geometries.[36] We instead attribute the faster ICD processes observed for the $2\ s^{-1}$ core-hole states of Na^+, Mg^{2+}, and Al^{3+} relative to the $2p^{-1}$ core-hole states of K^+ and Ca^{2+} to internal differences in the decay mechanisms of the ions.

In all the here discussed cases, ICD results in a *p*-type outer valence vacancy in the ion and an outer valence vacancy in the water environment. In the cases of Na^+, Mg^{2+}, and Al^{3+}, ICD starts with the dipole-allowed 2s → 2p transition where the involved orbitals belong to the same electronic shell allowing a much higher orbital overlap and thus a higher decay rate. In contrast, the initial transition in the K^+ and Ca^{2+} ions is a dipole-forbidden 2p → 3p one, involving the orbitals from different electronic shells. The difference between the slower $2p^{-1}$ decays of K^+ and Ca^{2+} and the faster $2s^{-1}$ decays of Na^+, Mg^{2+}, and Al^{3+} is thus reminiscent of the difference between the slower normal Auger decay and its faster special case, namely, the CK decay. Indeed, for ICD of inner-valence vacancies, it has been shown that dipole-forbidden transitions lead to much slower ICD decay compared to that involving dipole-allowed transitions.[46]

The rate difference between related Auger and CK processes is typically 1 order of magnitude. Our studies have shown that a similar rate difference exists between the normal and CK-type core level ICD processes. While for shallow core levels the Auger lifetimes are a few femtoseconds, the CK lifetimes are a few tenths of a femtosecond. The ICD lifetimes in aqueous ions are approximately of 1 and up to 2 orders of magnitude longer, namely, a few tens up to hundreds of femtoseconds for a normal core level ICD process and just a few femtoseconds for one of a CK-type.

■ CONCLUSION

The Ca^{2+} 2p core-hole decay spectrum of the aqueous $CaCl_2$ solution shows clear similarities to the K^+ 2p core-hole decay spectrum of the aqueous KCl solution.[12] The main features in these spectra correspond to the two-hole final states localized on

the metal ions. The spectra also exhibit weak features at higher KEs, related to the delocalized two-hole final states with vacancies, one in a solvated ion and the other in the neighboring water environment. Core level ICD-like processes lead to these states. By using the intensity ratio between the ICD and Auger spectral features and the core-hole clock method, the lifetimes of the ICD processes have been derived. Much insight into the dependence of the electronic decay processes on the ionic charge and size as well as on the ion−water separations has been gained by exploring the theoretical Auger spectra of the relevant microsolvated clusters. By comparing the theoretical spectra of microsolvated models with those of the bulk solutions, substantial impact of the water molecules beyond the first solvation shell on the chemical shifts and on the ICD efficiency, in particular in the case of the aqueous Ca^{2+} exhibiting a well structured second solvation shell, has been revealed. We have also compared the ICD lifetimes for the aqueous K^+ and Ca^{2+} with those of the aqueous Na^+, Mg^{2+}, and Al^{3+} reported in ref 18, and found 2 orders of magnitude difference which is attributed to different internal decay mechanisms. The Coster−Kronig-type core level ICD processes operating in the solvated Na^+, Mg^{2+}, and Al^{3+} ions involve dipole-allowed transitions in the atomic ions and are thus much more efficient than the normal core level ICD processes taking place in the solvated K^+ and Ca^{2+} which involve dipole-forbidden transitions.

■ ASSOCIATED CONTENT

Supporting Information. Details of calculations concerning cluster geometries, together with the complete refs 9, 11, 21, and 22. This material is available free of charge via the Internet at http://pubs.acs.org.

■ AUTHOR INFORMATION

Corresponding Author

nikolai.kryzhevoi@tc.pci.uni-heidelberg.de; olle.bjorneholm@fysik.uu.se

■ ACKNOWLEDGMENT

The Royal Thai Government and Nakhon Phanom University are grateful acknowledged for the graduate fellowship of W. Pokapanich. This work has been financially supported by the Swedish Reasearch Council (VR), the Göran Gustafsson foundation, the Knut and Alice Wallenberg foundation, the Carl Tryggers Foundation and the Deutsche Forschungsgemeinschaft. We also thank MAX lab staff for their assistance during the experments.

■ REFERENCES

(1) Cederbaum, L. S.; Zobeley, J.; Tarantelli, F. *Phys. Rev. Lett.* **1997**, *79*, 4778.

(2) Marburger, S.; Kugeler, O.; Hergenhahn, U.; Möller, T. *Phys. Rev. Lett.* **2003**, *90*, 203401.

(3) Jahnke, T.; Czasch, A.; Schöffler, M. S.; Schössler, S.; Knapp, A.; Käsz, M.; Titze, J.; Wimmer, C.; Kreidi, K.; Grisenti, R. E.; Staudte, A.; Jagutzki, O.; Hergenhahn, U.; Schmidt-Böcking, H.; Dörner, R. *Phys. Rev. Lett.* **2004**, *93*, 163401.

(4) Santra, R.; Zobeley, J.; Cederbaum, L. S. *Phys. Rev. B* **2001**, *64*, 245104.

(5) Öhrwall, G.; Tchaplyguine, M.; Lundwall, M.; Feifel, R.; Bergersen, H.; Rander, T.; Lindblad, A.; Schulz, J.; Peredkov, S.; Barth, S.; Marburger, S.; Hergenhahn, U.; Svensson, S.; Björneholm, O. *Phys. Rev. Lett.* **2004**, *93*, 173401.

(6) Lundwall, M.; Tchaplyguine, M.; Öhrwall, G.; Lindblad, A.; Peredkov, S.; Rander, T.; Svensson, S.; Björneholm, O. *Surf. Sci.* **2005**, *594*, 12.

(7) Mueller, I. B.; Cederbaum, L. S. *J. Chem. Phys.* **2006**, *125*, 204305.

(8) Mucke, M.; Braune, M.; Barth, S.; Förstel, M.; Lischke, T.; Ulrich, V.; Arion, T.; Becker, U.; Bradshaw, A.; Hergenhahn, U. *Nat. Phys.* **2010**, *6*, 143.

(9) Jahnke, T.; et al. *Nat. Phys.* **2010**, *6*, 139.

(10) Kryzhevoi, N. V.; Cederbaum, L. S. *Angew. Chem., Int. Ed.* **2011**, *50*, 1306.

(11) Öhrwall, G.; et al. *J. Chem. Phys.* **2005**, *123*, 054310.

(12) Pokapanich, W.; Bergersen, H.; Bradeanu, I. L.; Marinho, R. R. T.; Lindblad, A.; Legendre, S.; Rosso, A.; Svensson, S.; Björneholm, O.; Tchaplyguine, M.; Öhrwall, G.; Kryzhevoi, N. V.; Cederbaum, L. S. *J. Am. Chem. Soc.* **2009**, *131*, 7264–7271.

(13) Lindblad, A.; Bergersen, H.; Pokapanich, W.; Tchaplyguine, M.; Öhrwall, G.; Björneholm, O. *Phys. Chem. Chem. Phys.* **11**, **1758**, 2009.

(14) Kryzhevoi, N. V.; Cederbaum, L. S. *J. Phys. Chem. B* **2011**, *115*, 5441–5447.

(15) Brühwiler, P. A.; Karis, O.; Mårtensson, N. *Rev. Mod. Phys.* **2002**, *74*, 703.

(16) Björneholm, O.; Nilsson, A.; Sandell, A.; Hernnäs, B.; Mårtensson, N. *Phys. Rev. Lett.* **68, 1892**, 1992.

(17) Föhlisch, A.; Feulner, P.; Hennies, F.; Fink, A.; Menzel, D.; Sanchez-Portal, D.; Echenique, P. M.; Wurth, W. *Nature* **2005**, *436*, 373.

(18) Öhrwall, G.; Ottosson, N.; Pokapanich, W.; Legendre, S.; Svensson, S.; Björneholm, O. *J. Phys. Chem. B* **2010**, *114*, 17057.

(19) Winter, B.; Faubel, M. *Chem. Rev.* **2006**, *106*, 1176–1211.

(20) Weber, R.; Winter, B.; Schmidt, P. M.; Widdra, W.; Hertel, I. V.; Dittmar, M.; Faubel, M. *J. Phys. Chem. B* **2004**, *108*, 4729.

(21) Bässler, M.; et al. *J. Electron Spectrosc. Relat. Phenom.* **1999**, *101−103*, 953.

(22) Bässler, M.; et al. *Nucl. Instrum. Methods Phys. Res., Sect. A* **2001**, *469*, 382.

(23) Bergersen, H.; Marinho, R. R. T.; Pokapanich, W.; Lindblad, A.; Björneholm, O.; Sæthre, L. J.; Öhrwall, G. *J. Phys.: Condens. Matter* **2007**, *19*, 326101.

(24) Blaudeau, J.-P.; McGrath, M. P.; Curtiss, L. A.; Radom, L. *J. Chem. Phys.* **1997**, *107*, 5016.

(25) Schirmer, J.; Barth, A. *Z. Phys. A* **1984**, *317*, 267.

(26) Tarantelli, F. *Chem. Phys.* **2006**, *329*, 11.

(27) Pacios, L. F.; Christiansen, P. A. *J. Chem. Phys.* **1985**, *82*, 2664.

(28) Hurley, M. M.; Pacios, L. F.; Christiansen, P. A.; Ross, R. B.; Ermler, W. C. *J. Chem. Phys.* **1986**, *84*, 6840.

(29) Dunning, T. H., Jr. *J. Chem. Phys.* **1989**, *90*, 1007.

(30) Tarantelli, F.; Sgamelloti, A.; Cederbaum, L. S. *J. Chem. Phys.* **1991**, *94*, 523.

(31) Elango, M.; Ausmees, A.; Kikas, A.; Nõmmiste, E.; Ruus, R.; Saar, A.; van Acker, F. J.; Andersen, J. N.; Nyholm, R.; Martinson, I. *Phys. Rev. B.* **1993**, *47*, 11736.

(32) Kikas, A.; Ausmees, A.; Elango, M.; Nõmmiste, E.; Ruus, R.; Saar, A. *J. Electron Spectrosc. Relat. Phenom.* **1994**, *68*, 287.

(33) Fulton, J. L.; Heald, S. M.; Badyal, Y. S.; Simonson, J. M. *J. Phys. Chem. A* **2003**, *107*, 4688.

(34) Badyal, Y. S.; Barnes, A. C.; Cuello, G. J.; Simonson, J. M. *J. Phys. Chem. A* **2004**, *108*, 11819.

(35) Jalilehvand, F.; Spångberg, D.; Lindqvist-Reis, P.; Hermansson, K.; Persson, I.; Sandström, M. *J. Am. Chem. Soc.* **2001**, *123* (3), 431.

(36) Marcus, Y. *Chem. Rev.* **2009**, *109*, 1346.

(37) Smirnov, P. R.; Trostin, V. N. *Russ. J. Gen. Chem.* **2009**, *79*, 1600.

(38) Soper, A. K.; Weckström, K. *Biophys. Chem.* **2006**, *124*, 180.

(39) Glezakou, V.-A.; Chen, Y.; Fulton, J. L.; Schenter, G. K.; Dang, L. X. *Theor. Chem. Acc.* **2006**, *115*, 86.

(40) Smirnov, P. R.; Trostin, V. N. *Russ. J. Gen. Chem.* **2101**, *77*, 1600.
(41) Almbladh, C.-O.; Morales, A. L. *Phys. Rev. B* **1989**, *39*, 3503.
(42) Kukk, E.; Huttula, M.; Aksela, H.; Aksela, S.; Nõmmiste, E.; Kikas, A. *J. Phys. B* **2003**, *36*, L85.
(43) Kryzhevoi, N. V.; Averbukh, V.; Cederbaum, L. S. *Phys. Rev. B* **2007**, *76*, 094513.
(44) Pauling, L. *J. Am. Chem. Soc.* **1947**, *69*, 542–553.
(45) Slater, J. C. *J. Chem. Phys.* **1964**, *41*, 3199–3204.
(46) Averbukh, V.; Müller, I. B.; Cederbaum, L. S. *Phys. Rev. Lett.* **2004**, *93*, 263002.